TWENTY FIRST EUROPEAN ROTORCRAFT FORUM

Paper No VI.6

ANALYSIS OF TORSIONAL MOMENTS PRODUCED IN MAIN ROTOR BLADES AND RESULTS OBTAINED

N.S.Pavlenko, A.Y.Barinov

MIL MOSCOW HELICOPTER PLANT

RUSSIA

August 30 - September 1, 1995

SAINT - PETERSBURG, RUSSIA

Paper nr.: VI.6

Analysis of Torsion Moments Produced in Main Rotor Blades and Results Obtained.

N.S. Pavlenko; A.Yu. Barinov

TWENTY FIRST EUROPEAN ROTORCRAFT FORUM
August 30 - September 1, 1995 Saint-Petersburg, Russia

Analysis of Torsional Moments Produced in Main Rotor Blades and Results Obtained.

N.S. Pavlenko
Deputy Head of Structural Department
and
A.Yu. Barinov
Design Engineer

Mil Helicopter Plant
Russia

This paper presents analytical procedures used to calculate bending and torsional moments produced on the blade subject to forced oscillations, as well as moments produced on the swashplate.

The procedures described here allow us to determine aerodynamic performance, blade flap and lag deflection, as well as torsional deflection and their respective bending and torsional moments with their harmonic content for main rotors having elastic blades undergoing flap bending, lag bending and elastic twist, articulated, rigid blade root attachments; for sophisticated hub designs intended for modern semirigid and rigid rotors incorporating flexure elements, control fairings and elastomeric or hydraulic dampers; as well as for blades having straight, swept and anhedral tips.

Analytical Procedures

Helicopter blade low oscillations of the rotating main rotor are described by a system of partial differential equations of the fourth order that can be presented in the operator form as follows:

$$L\,[q(r,t)] = F \qquad (1)$$

Here L is the operator of the system including three partial differential equations relative to unknown functions q(r,t) and the required boundary conditions.

$$q(r,t) = \begin{vmatrix} x \\ y \\ \varphi \end{vmatrix}$$

where
- q is column matrix of the generalized coordinates;
- x is inplane blade deflection (deformation);
- y is blade deflection (deformation) in the plane containing the axis of rotation of the rotor;
- φ is blade torsional deflection and deformation relative its longitudinal axis;
- F is external aerodynamic forces.

The anhedral-tip blade is taken into account in the following way. Let us denote all the parameters of the blade elastic axis junction point by adding the sign (*) to the appropriate symbol. When passing over the elastic axis junction point, it is necessary to satisfy the conditions of geometric conjugation of the elements which further will be designated as blade and tip elements. Besides, additional terms will appear in the formulas used for inertia and aerodynamic loads as compared to the sraight-tip blade.

Let us introduce right-hand coordinate systems.

$O_1x_1y_1z_1$ is the coordinate system related to the undeformed blade. The O_1z_1 axis is directed along the blade radius, while the O_1y_1 axis coincides with the main rotor mast axis.

$O_2x_2y_2z_2$ is the coordinate system originating in the elastic axis junction point, and the coordinate axes are parallel to the axes of the $O_1x_1y_1z_1$ system.

$O_2'x_2'y_2'z_2'$ is the coordinate system in which the $O_2'y_2'$ axis coincides with the O_2y_2 axis, and the angle between the O_2z_2 and $O_2'z_2'$ axes is equal to the angle of deflection of the section at the $(x')^*$ elastic axis junction point with the blade bending in the plane of the maximum stiffness.

$O_3x_3y_3z_3$ is the coordinate system in which the O_3x_3 axis coincides with the O_2x_2 axis and the angle between the O_3z_3 and O_2z_2 axes is equal to the angle of deflection of the section at the $(y')^*$ elastic axis junction point with the blade bending in the plane of the minimum stiffness.

$O_4x_4y_4z_4$ is the coordinate system in which the O_4z_4 and O_3z_3 axes coincide with each other, the O_4x_4 axis is at the ϕ^* angle denoting blade elastic twist at the junction point relative to the O_3x_3 axis.

$O_5x_5y_5z_5$ is the coordinate system in which the angle between the O_5z_5 and O_4z_4 axes is equal to the tip sweep angle χ_ξ (the sweptback angle is considered to be positive), and the O_5y_5 and O_4y_4 axis coincide with each other.

$O_6x_6y_6z_6$ is the coordinate system for which the O_6x_6 axis coincides with the O_5x_5 axis, and the O_6y_6 axis is at the χ_β angle relative to the O_5y_5 axis. The anhedral angle is assumed to be positive.

The origin of the $O_2'x_2'y_2'z_2'$ $O_3x_3y_3z_3$, $O_4x_4y_4z_4$, $O_5x_5y_5z_5$, $O_6x_6y_6z_6$ coordinate systems coincides with that of the $O_2x_2y_2z_2$ coordinate system.

Sequential transformation of projections of some vector from the $O_2x_2y_2z_2$ coordinate system into $O_2'x_2'y_2'z_2'$, $O_3x_3y_3z_3$, $O_4x_4y_4z_4$, $O_5x_5y_5z_5$ and $O_6x_6y_6z_6$ systems is carried out by matrices

$$A_{22'} = \begin{vmatrix} \cos x'_* & 0 & -\sin x'_* \\ 0 & 1 & 0 \\ \sin x'_* & 0 & \cos x'_* \end{vmatrix};$$

$$A_{2'3} = \begin{vmatrix} 1 & 0 & 0 \\ 0 & \cos y'_* & -\sin y'_* \\ 0 & \sin y'_* & \cos y'_* \end{vmatrix};$$

$$A_{34} = \begin{vmatrix} \cos\varphi_* & -\sin\varphi_* & 0 \\ \sin\varphi_* & \cos\varphi_* & 0 \\ 0 & 0 & 1 \end{vmatrix};$$

$$A_{45} = \begin{vmatrix} \cos\chi_\xi & 0 & -\sin\chi_\xi \\ 0 & 1 & 0 \\ \sin\chi_\xi & 0 & \cos\chi_\xi \end{vmatrix};$$

$$A_{56} = \begin{vmatrix} 1 & 0 & 0 \\ 0 & \cos\chi_\beta & \sin\chi_\beta \\ 0 & -\sin\chi_\beta & \cos\chi_\beta \end{vmatrix};$$

By multiplying matrices $A_{22'}$, $A_{2'3}$, A_{34}, A_{45} and A_{56}, we can obtain the transformation matrix to convert the $O_2x_2y_2z_2$ coordinate system into the $O_6x_6y_6z_6$, coordinate system which (considering that the $(y')^*$, $(x')^*$ and ϕ^* angles are small and ignoring values of less than the second order) can be written as

$$A_{26} = A_{22'} \cdot A_{2'3} \cdot A_{34} \cdot A_{45} \cdot A_{56} =$$

$$= \begin{vmatrix} \cos\chi_\xi - x'_*\sin\chi_\xi & -\varphi_*\cos\chi_\beta + \sin\chi_\beta(\sin\chi_\xi + x'_*\cos\chi_\xi) & -\varphi_*\sin\chi_\beta - \cos\chi_\beta(\sin\chi_\xi + x'_*\cos\chi_\xi) \\ \varphi_*\cos\chi_\xi - y'_*\sin\chi_\xi & \cos\chi_\beta + \sin\chi_\beta(\varphi_*\sin\chi_\xi + y'_*\cos\chi_\xi) & \sin\chi_\beta - \cos\chi_\beta(\varphi_*\sin\chi_\xi + y'_*\cos\chi_\xi) \\ x'_*\cos\chi_\xi + \sin\chi_\xi & y'_*\cos\chi_\beta + \sin\chi_\beta(x'_*\sin\chi_\xi - \cos\chi_\xi) & y'_*\sin\chi_\beta - \cos\chi_\beta(x'_*\sin\chi_\xi - \cos\chi_\xi) \end{vmatrix}$$

Conversion from the tip axes to the $O_2x_2y_2z_2$ axes is accomplished with the help of inverse matrix A^{-1}_{22}, which is equal to transposed matrix A^{T}_{22}.

Let us introduce the following expressions:

$$\bar{q}_6 = \begin{vmatrix} x_6 \\ y_6 \\ z_6 \end{vmatrix}; \quad \bar{h} = \begin{vmatrix} x_* \\ y_* \\ z_* \end{vmatrix}$$

Now the coordinates of any tip point after the blade deflection are expressed in the $O_1x_1y_1z_1$ system:

$$\bar{q}_1 = A_{26}^T \cdot \bar{q}_6 + \bar{h} \qquad (2)$$

From equation (2) conditions of geometric conjugation can be obtained.

Conjugation conditions for inner force factors follow from the equation below:

$$\bar{q}_{M3} = A_{36}^T \cdot \bar{q}_{M6} \qquad (3)$$

Here the following expressions are introduced:

$$A_{36}^T = [A_{34} A_{45} A_{56}]^T;$$

$$\bar{q}_{M3} = \begin{vmatrix} M_3^F \\ M_3^L \\ M_3^T \end{vmatrix}; \quad \bar{q}_{M6} = \begin{vmatrix} M_6^F \\ M_{36}^L \\ M_{36}^T \end{vmatrix};$$

Projections of the bending and torsional moments actingin the blade section along the Ojxj, Ojyj and Ojzj can be expressed in terms of $M^F j$, $M^L j$ and $M^T j$ respectively, where j is the index of the Ojxjyjzj coordinate system.

From equation (3) formulas for projections of the bending and torsional moments on the O_3x_3, O_3y_3 and O_3z_3 axes are obtained.

When conditions (2) and (3) in equations of blade coupled bending and torsional oscillations are met, the blade swept and anhedral tips are taken into account.

In system of equations (1) blade flap and lag bending and torsional deflections are considered to be the **q(r,t)** generalized coordinates. Each generalized coordinate is a function of two independent variables: radius and time.

Solutions of system (1) are presented in the form of series expansion in normal modes for coupled bending and torsional oscillations in the two planes:

$$q(r,t) = \sum_j \delta_j \, q_j \qquad (4)$$

where **j=1,2,3...** the number of normal modes to be assumed in the analysis;

q_j means the form component of the j-th tone of the blade eigenfrequency in emptiness which is the function of its radius;

δ_j means some time functions which are called deflection coefficients.

The q_j normal modes are determined from system of differential equations (1) when its right side is equal to zero.

In the analysis the blade is presented as a beam model divided into z elements. The weight of each element is concentrated at its ends as discrete masses. Stiffness characteristics are presented as step lines so that they could have constant values within each element. Having applied the Galerkin approach to system of partial differential equations (1), we obtain a system of differential equations of the second order relative to δj deflection coefficients.

$$\ddot{\delta}_j + p_j \cdot \delta_j = A_j \qquad (5)$$

Here p_j is the frequency of blade natural coupled oscillations in the j-th tone;

A_j is the work of the aerodynamic forces during their displacement along the j-th generalized coordinate that is divided by the blade equivalent mass .

The order of system (5) is determined by the number of the series terms in the expansion of solution (4).

Calculations of the aerodynamic forces comprising the right part of system (5) are performed by using lift, drag and torque coefficients [(Cy), (Cx),(mz) respectively] that are functions of the blade airfoil angle of attack and Mach number obtained from wind tunnel test results.

Induced velocity is assumed to be constant over the rotor disc or it is calculated by using the vortex theory.

The δj deflection coefficients can be calculated by using numerical integration of system of equations (5).

Calculation Results

Using the above procedures, torsional and bending moments on the main rotor blades for helicopter of different weight categories (light, medium and heavy-lift) were calculated (Table 1).

Table 1

Helicopter	TOW kg	Main rotor diameter m	Number of blades
Mi-34	1,350	10.0	4
Mi-28	11,000	17.3	5
Mi-8	12,000	21.0	5
Mi-26	56,000	32.0	8

The calculations were made for straight-tip and swept-tip blades.

The paper gives some results of these calculations and their comparison with flight test data.

The most complicated thing in calculating torsional moments is proper azimuth distribution of torsional moment values, their phase, amplitude and harmonic content for each flight condition.

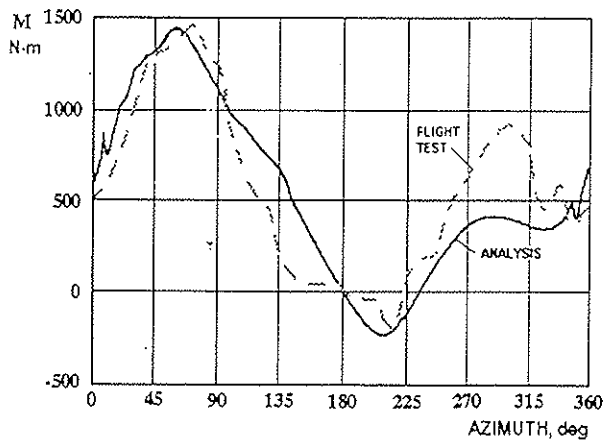

Fig.1 Mi-28 helicopter torsional moment versus blade azimuth, 250 km/h (IAS).

Fig.1 shows torsional moment versus azimuth for the Mi-28 main rotor blade at an airspeed of 250 km/h. The same dependence obtained from flight measurements is given here. It can be seen from the diagram that the calculated data are in good agreement with the flight test results.

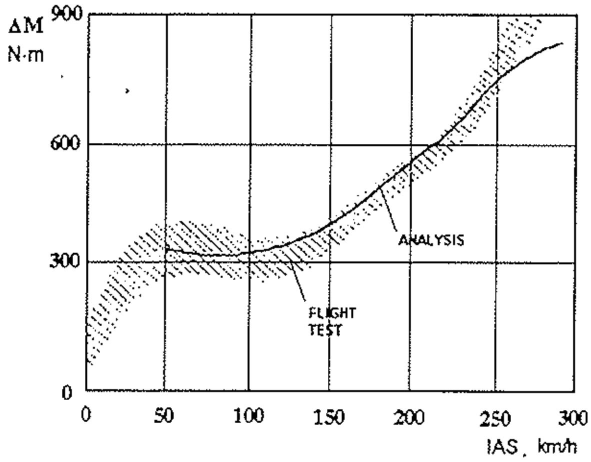

Fig.2 Mi-28 helicopter torsional moment amplitude versus airspeed.

The solid line in the diagram in Fig.2 shows torsional moment amplitude versus the Mi-28 airspeed. The hatching shows the area of values obtained in flight measurements. Here good agreement of the calculated and experimental data can be seen within the whole airspeed range with the exception of flight at airspeeds close to the maximum value and hovering. It can be attributed to the influence of stall.

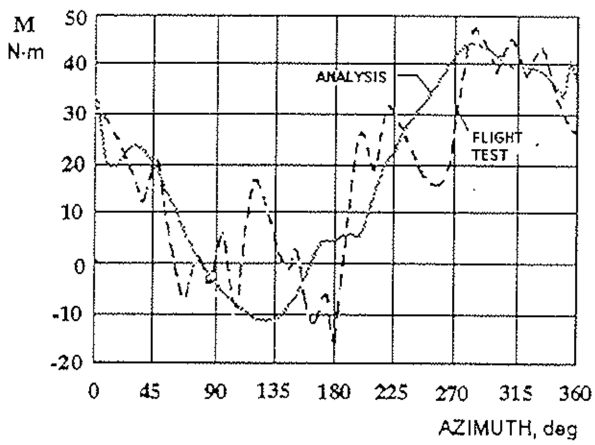

Fig.3 Mi-34 helicopter torsional moment versus blade azimuth, 100 km/h (IAS).

Fig.3 shows torsional moment versus blade azimuth for the Mi-34 helicopter.

In this case the flight condition which is characterized by high harmonics was analysed (the diagram is a copy of the oscillogram). This is mainly attributed to the engine and blade features. The engine features are not taken into account, as for the blade features, they can be considered by taking a greater number of the series terms and a more sophisticated model of aerodynamic forces in the analysis. But, as can be seen from the diagram, calculations are in good agreement with the experiment for low harmonics. Here, different dependences of the torsional moment on the blade azimuth for the Mi-34 and Mi-28 as well as their proper simulation by analysis should be noted.

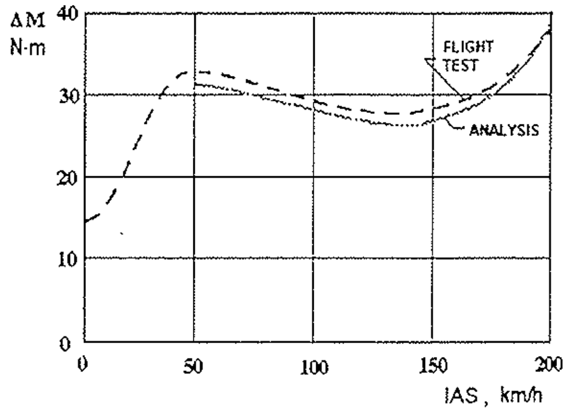

Fig.4 Mi-34 helicopter torsional moment amplitude versus airspeed.

The diagram in Fig. 4 presents the torsional moment amplitude versus airspeeds and a good agreement of calculated and flight data (the exception is hovering and low-speed flight).

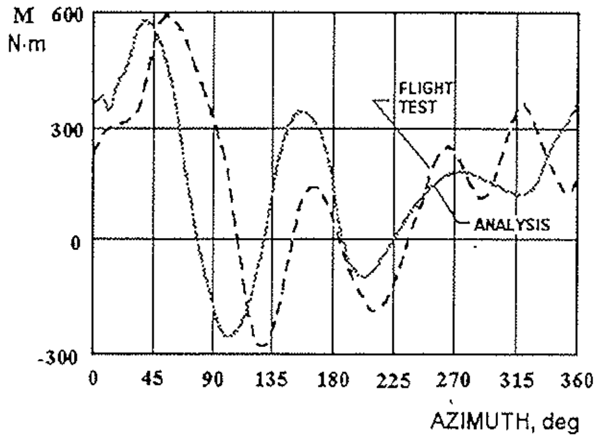

Fig.5 Mi-8 helicopter torsional moment versus blade azimuth, 240 km/h (IAS).

Fig.5 gives torsional moment versus blade azimuth for the Mi-8 main rotor at an airspeed of 240 km/h. Here we have good convergence of calculated data and flight measurements. In this case the law governing the torsional moment change with azimuth differs greatly from that for the Mi-28 and the Mi-34. Here high harmonics were obtained by analysis as can be seen in the diagram.

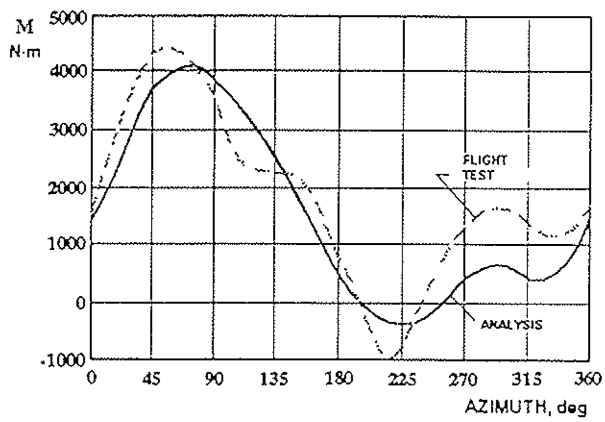

Fig.6 Mi-26 helicopter torsional moment versus blade azimuth, 280 km/h (IAS).

Fig.6 shows torsional moment versus blade azimuth for the Mi-26 heavy-lift helicopter that was obtained by analysis and by flight test results. Good agreement between the calculation and experiment is clearly seen.

When comparing the azimuth distribution of torsional moments for different helicopters (Table 1), general regularities should be noted inherent in these dependences, and regularities that actually do not depend upon the type of helicopter or the main rotor configuration. Thus, all the diagrams of the torsional moment functions have a local maximum in the vicinity of azimuth equal to $\pi/6$. The only exception is the torsional moment curve for the Mi-34 helicopter: in this case this maximum is shifted into a lower azimuth value. In some azimuth area close to π the torsional moment curves have a local minimum. In the region of azimuth equal to $3/4\pi$ there is another local minimum.

The torsional moment curves shown in the diagrams for the main rotor blades of different helicopters differ substantially. For the Mi-26 and Mi-28 helicopters the harmonic composition of the torsional moment is similar and has an insignificant content of high harmonics. The torsional moment versus blade azimuth curve for the Mi-8 helicopter contains quite a large 4/rev content, and that for the Mi-34, harmonics influenced by the engine and blade features.

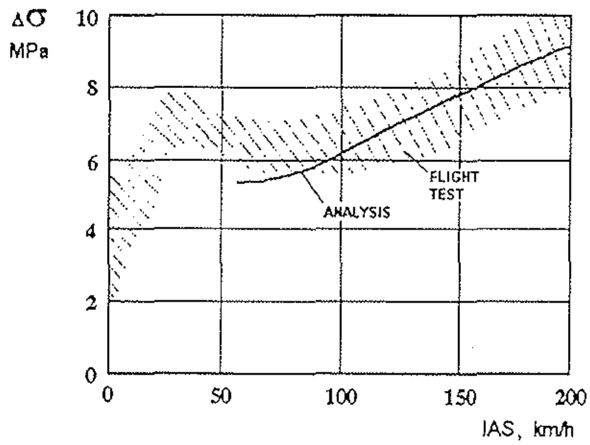

Fig.7 Mi-34 helicopter alternating stresses in the plane of minimum stiffness ($\Delta\sigma$) versus airspeed.

The diagram in Fig.7 shows variation of alternating stresses in the Mi-34 main rotor blade spar in the plane of the minimum stiffness. It is clearly seen from the diagram that in the region of average speeds there is a good agreement between the calculated and experimental data. The exception is an area of low-speed flight; to make calculations in this particular area it is necessary to use more sophisticated vortex models.

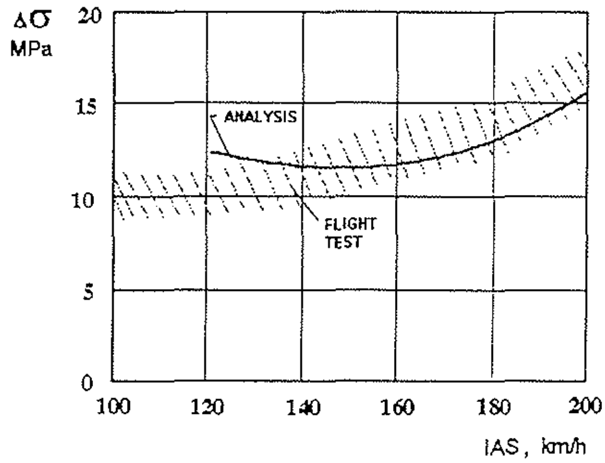

Fig.8 Mi-34 helicopter alternating stresses in the plane of maximum stiffness ($\Delta\sigma$) versus airspeed.

Fig.8 presents comparison of analytical data with measurements made in flight tests for alternating stresses in the blade spar acting in the plane of the maximum stiffness. Here we also have a good agreement between calculated and experimental data for average airspeeds, and an unsatisfactory one for low airspeeds and deceleration.

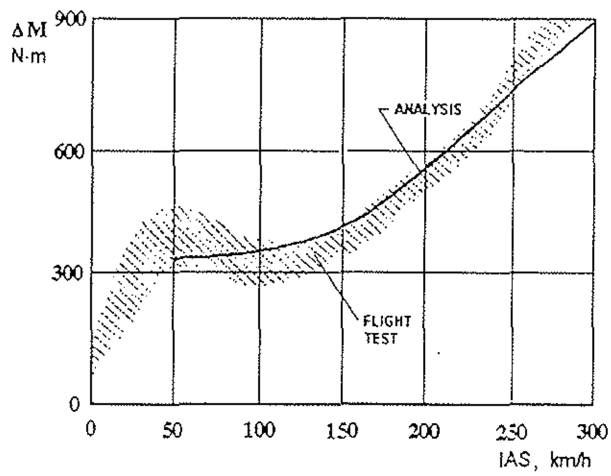

Fig.9 Mi-28 helicopter torsional moment amplitude versus airspeed.

Fig.9 shows the calculated torsional moment amplitude versus airspeed for the swept-tip blade of one and the same helicopter. A set of the Mi-28 main rotor swept-tip blades underwent comprehensive flight tests during which blade and control system loads were measured. The measurements showed that the torsional moment amplitude was slightly higher on the swept-tip blade at average airspeeds of 120-220 km/h as compared to the straight-tip blade. But at airspeeds of 230 km/h and higher torsional moments (therefore swashplate loads) for the swept-tip blade were smaller. That was the main reason for using swept-tip blades in the Mi-28 main rotor.

Conclusions

1. Analytical procedures for calculating torsional and bending moments acting on the helicopter main rotor blade have been developed. Comparison of calculated data with those obtained from flight tests of the Mi-34, Mi-28, Mi-8 and Mi-26 helicopters has been made.

2. Calculations of torsional moments for the Mi-28 swept-tip main rotor blade have been made. Comparison with flight test results for the swept-tip blade has been drawn.

Calculated data are in good agreement with the flight test results for average airspeeds.